Enhancement of Pure Spin Currents in Spin Pumping $Y_3Fe_5O_{12}$/Cu/Metal Trilayers through Spin Conductance Matching

Chunhui Du, Hailong Wang, Fengyuan Yang,* and P. Chris Hammel†

Department of Physics, The Ohio State University, Columbus, Ohio 43210, USA

(Received 18 March 2014; published 15 May 2014)

Spin transport efficiency in heterostructures depends on the spin conductances of each constituent and their interfaces. We report a comparative study of spin pumping in $Y_3Fe_5O_{12}$/Cu/Pt and $Y_3Fe_5O_{12}$/Cu/W trilayers. Surprisingly, the insertion of a Cu interlayer between $Y_3Fe_5O_{12}$ and W substantially improves (over a factor of 4) the spin current injection into W while similar insertion between $Y_3Fe_5O_{12}$ and Pt degrades the spin current. This is a consequence of a much improved $Y_3Fe_5O_{12}$/Cu spin mixing conductance relative to that for $Y_3Fe_5O_{12}$/W. This result implies the possibility of engineered heterostructures with matching spin conductances to enable optimal spin transport efficiency.

DOI: 10.1103/PhysRevApplied.1.044004

Conventional electronic devices operate via flow of electrical charges. The decoupling of spin and charge currents in ferromagnetic resonance (FMR) driven spin pumping offers the potential to enable low energy cost, high efficiency spintronics with implications for both next generation computing [1,2] and global energy consumption [3]. Spin pumping, driven thermally as well as by FMR, is being widely used to generate pure spin currents from ferromagnets (FM) into normal metals (NM) [4–18]. The efficiency of spin pumping is largely determined by the spin mixing conductance $g_{\uparrow\downarrow}$ [4,5] of the FM/NM interface. Typically, the NM is chosen to be a spin sink—Pt, W, or Ta with large inverse spin Hall effect (ISHE), while lighter metals such as Cu are rarely used. Various FM/NM or FM/NM_1/NM_2 structures have been extensively studied by both FMR spin pumping [6–16] and spin Seebeck measurements [17,18]. Because of its low magnetic damping and insulating nature, $Y_3Fe_5O_{12}$ (YIG) is very attractive for microwave applications and spin pumping [6,7,11–13,15,18–21]. It will be important to understand the spin transmissivity of multilayers in order to enable the use of intervening layers for optimizing spin transport properties. Cu interlayers were recently used to eliminate proximity induced ferromagnetism in YIG/Pt [18,22–24]. A quantitative understanding of spin current generation and transport in YIG/Cu and YIG/Cu/NM heterostructures, especially the spin mixing or spin conductance at each interface, is still lacking.

We use epitaxial YIG (20 nm) films grown on $Gd_3Ga_5O_{12}$ (111) by off-axis sputtering; these films enable mV-level ISHE voltages in YIG/Pt and YIG/W spin pumping measurements [11,12,25]. Figure 1(a) shows an x-ray diffraction (XRD) scan of a YIG film with clear Laue oscillations and a rocking curve full width at half maximum (FWHM) of 0.0073° [inset to Fig. 1(a)]. Figures 1(b)–1(d) show atomic force microscopy (AFM) images of a 20-nm YIG film, a YIG/Cu(5 nm) and a YIG/Cu(20 nm) bilayer with a root-mean-square (rms) roughness of 0.15, 0.19, and 0.22 nm, respectively, indicating the smooth surfaces of the YIG films and the Cu layers.

Our FMR ($f = 9.65$ GHz) spin pumping measurements are performed at room temperature on YIG(20 nm)/Cu(t_{Cu})/Pt(5 nm) and YIG(20 nm)/Cu(t_{Cu})/W(5 nm) trilayers where the Cu thickness t_{Cu} is varied from 0 to 20 nm. All metal layers are deposited by off-axis, ultrahigh vacuum sputtering [11,12,25]. Samples approximately 1 mm wide and approximately 5 mm long are placed in

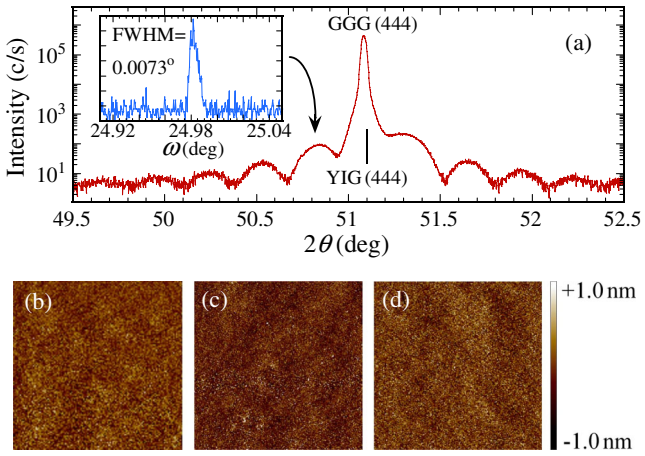

FIG. 1. (a) θ–2θ XRD scan of a 20-nm thick YIG film on GGG (111), which exhibits clear Laue oscillations. Inset: rocking curve of the first satellite peak on the left of YIG (444) peak with FWHM of 0.0073°. AFM images of (b) a 20-nm bare YIG film, (c) a YIG/Cu (5 nm) bilayer, and (d) a YIG/Cu (20 nm) bilayers over an area of 10 μm × 10 μm with an rms roughness of 0.15, 0.19, and 0.22 nm, respectively.

*fyyang@physics.osu.edu
†hammel@physics.osu.edu

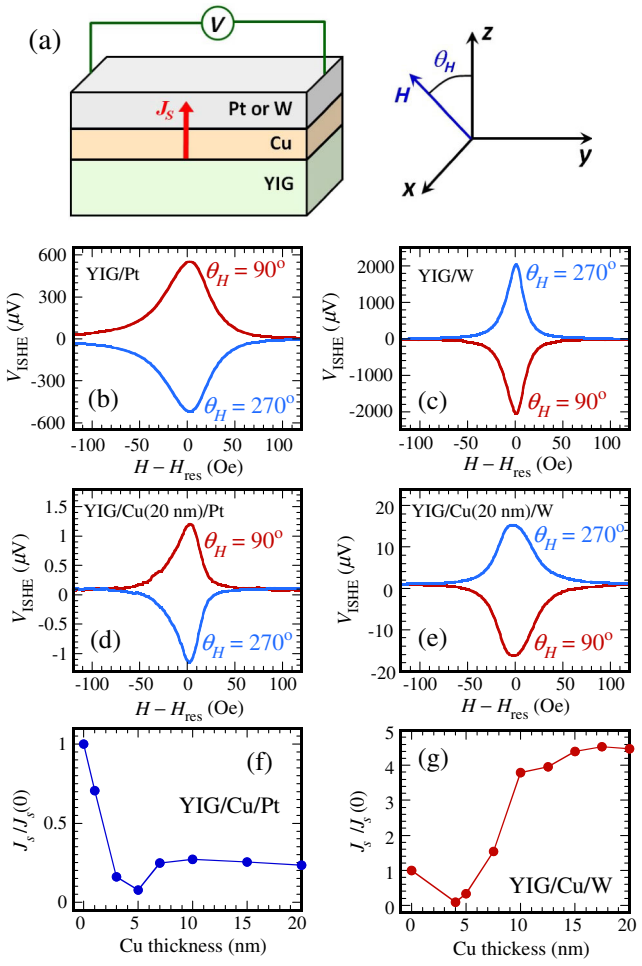

FIG. 2. (a) Schematic of experimental geometry for ISHE voltage measurements and V_{ISHE} vs $H - H_{res}$ spectra of (b) a YIG/Pt bilayer, (c) a YIG/W bilayer, (d) a YIG/Cu(20 nm)/Pt trilayer, and (e) a YIG/Cu(20 nm)/W trilayer at $\theta_H = 90°$ and 270° (in-plane fields). The thicknesses of all YIG, Pt, and W layers are 20, 5, and 5 nm, respectively. Spin current J_s in (f) YIG/Cu/Pt and (g) YIG/Cu/W trilayers normalized to $J_s(0)$ in YIG/Pt and YIG/W bilayers, respectively, as a function of the Cu thickness.

the center of an FMR cavity in a dc magnetic field ($\boldsymbol{H}$) applied in the xz plane, as shown in the schematic in Fig. 2(a). At resonance the precessing YIG magnetization transfers angular momentum to the conduction electrons in Cu. Since t_{Cu} is much smaller than the spin diffusion length (λ_{SD}), spin accumulation in the Cu spacer drives a spin current J_s into the Pt or W layer. As a consequence of the ISHE, the spin current J_s into the Pt or W is converted into a charge current, resulting in a voltage (V_{ISHE}) along the y axis. Figures 2(b) and 2(c) show V_{ISHE} vs $H - H_{res}$ spectra, where H_{res} is the resonance field of YIG, for YIG/Pt and YIG/W bilayers at $\theta_H = 90°$ and 270° (both in-plane fields) at rf input power $P_{rf} = 200$ mW, which gives $V_{ISHE} = 552\ \mu$V and -2.04 mV, respectively. The sign reversal for YIG/W reflects the opposite spin Hall angles of W and Pt. Figures 2(d) and 2(e) show the V_{ISHE} vs $H - H_{res}$ spectra for YIG/Cu(20 nm)/Pt and YIG/Cu(20 nm)/W trilayers. The peak values decrease to $V_{ISHE} = 1.21$ and $-16.3\ \mu$V as compared to YIG/Pt and YIG/W with direct contact, respectively.

To compare the effect of the Cu spacer on J_s, the spin current detected in Pt or W in the two trilayer systems, we show in Figs. 2(f) and 2(g) the t_{Cu} dependence of J_s normalized by $J_s(0)$, the spin current detected in the YIG/Pt and YIG/W bilayers without the Cu interlayer. Spin current J_s can be calculated from [26,27]

$$J_s = \frac{2e}{\hbar}\frac{V_{ISHE}}{\theta_{SH}\lambda_{SD}\tanh(\frac{t_{NM}}{2\lambda_{SD}})wR}, \tag{1}$$

where t_{NM} and θ_{SH} are the thickness and spin Hall angle of Pt or W, R and w the total resistance and width of the trilayers, respectively. The total resistance for the YIG/Pt bilayer sample is 487.4 Ω. As the Cu interlayer is inserted between YIG and Pt with increasing thickness, the total resistance R decreases and reaches 7.7 Ω at 20-nm Cu due to the shunting effect of Cu. For the YIG/W bilayer, the resistance is 6045.6 Ω, while it decreases to 9.3 Ω for the YIG/Cu(20 nm)/W trilayer. We note that the term $\theta_{SH}\lambda_{SD}\tanh(\frac{t_{NM}}{2\lambda_{SD}})$ in Eq. 1 is canceled in the normalized spin current $J_s/J_s(0)$. Taking the variation of total resistance R and width w into account, we show in Figs. 2(f) and 2(g) that with the insertion of Cu, the normalized spin current $J_s/J_s(0)$ initially decreases dramatically at $t_{Cu} \leq 5$ nm, then increases and eventually reaches a plateau at $t_{Cu} \geq 10$ nm. However, YIG/Cu/Pt and YIG/Cu/W show opposite plateau values of $J_s/J_s(0)$: for YIG/Cu/Pt, J_s is only about 20%–25% of J_s (0), while for YIG/Cu/W, J_s is 4.5 times $J_s(0)$. The initial decrease of J_s at $t_{Cu} \leq 5$ nm may be related to the much higher resistivity of thin Cu layers due to finite size effect which could induce significant spin flipping [4,5]. At $t_{Cu} \geq 10$ nm, the resistivity of Cu layers decreases significantly and spin accumulation in Cu occurs. A fraction of the accumulated spins in Cu diffuse back into YIG while the remainder is transmitted into the Pt or W, producing an ISHE signal. The ratio between these two fractions is determined by the interfacial spin mixing conductances $g^{\uparrow\downarrow}_{YIG/Cu}$ and spin conductance $g_{Cu/Pt}$ and $g_{Cu/W}$.

To uncover the mechanism behind the different spin pumping behavior of the two trilayer systems, we need to determine the spin mixing conductances from the enhancement of Gilbert damping α due to spin pumping. We obtain α by measuring the frequency dependencies of the FMR linewidth ΔH using a broadband microstrip transmission line. In all cases the linewidth increases linearly with frequency from 10 to 20 GHz (Fig. 3) following [28],

$$\Delta H = \Delta H_{inh} + \frac{4\pi\alpha f}{\sqrt{3}\gamma}, \tag{2}$$

where $\Delta H_{\rm inh}$ is the inhomogeneous broadening and γ is the gyromagnetic ratio. We define the enhancement of Gilbert damping due to spin pumping, $\alpha_{\rm sp} = \alpha_{\rm YIG/Cu/NM} - \alpha_{\rm YIG}$ for trilayers and $\alpha_{\rm sp} = \alpha_{\rm YIG/NM} - \alpha_{\rm YIG}$ for bilayers.

Figure 3(a) and Table I show that $\alpha_{\rm sp} = (2.1 \pm 0.1) \times 10^{-3}$ for YIG/Pt approximately doubles that for YIG/Cu(20 nm)/Pt, $(1.1 \pm 0.1) \times 10^{-3}$, in agreement with the previous study on Py/Cu/Pt [14] and YIG/Cu/Pt multilayers [23]. However, the order is reversed for YIG/Cu/W: $\alpha_{\rm sp} = (2.1 \pm 0.2) \times 10^{-3}$ for YIG/Cu(20 nm)/W is more than 3 times larger than the value of $(6.3 \pm 0.6) \times 10^{-4}$ for YIG/W [Fig. 3(b)]. Cavity FMR measurements also confirm this trend as shown in Figs. 3(d) and 3(e). The linewidth change for YIG/Cu(20 nm)/Pt compared to the bare YIG is 6.0 Oe which is smaller than the value of 12.6 Oe for YIG/Pt. However, for YIG/Cu(20 nm)/W trilayer, the linewidth change is 13.1 Oe which is larger than the value of 6.4 Oe for YIG/W. This implies a significant difference at the interfaces in YIG/Cu/Pt and YIG/Cu/W compared to YIG/Pt and YIG/W. In order to understand this behavior, we need to determine the spin mixing conductances of $g^{\uparrow\downarrow}_{\rm YIG/Cu}$, $g^{\uparrow\downarrow}_{\rm YIG/Pt}$, and $g^{\uparrow\downarrow}_{\rm YIG/W}$, and the spin conductances of $g_{\rm Cu/Pt}$ and $g_{\rm Cu/W}$.

Tserkovnyak *et al.* provide a theory for quantitative analysis of interfacial spin mixing conductance [4,5] for metallic FM/NM bilayers or trilayers where the real part of $g_{\uparrow\downarrow}$ is dominant. For YIG/NM interfaces, it has been reported recently that the imaginary part of $g_{\uparrow\downarrow}$ is also negligibly small [29,30]. Thus, this theory is applicable for YIG/NM systems as well. The spin pumping induced Gilbert damping enhancement can be expressed as [4,5,7,31–33]

$$\alpha_{\rm sp} = \frac{g\mu_{\rm B}}{4\pi M_s t_{\rm YIG}} g^{\uparrow\downarrow}_{\rm eff}, \tag{3}$$

where $g^{\uparrow\downarrow}_{\rm eff}$ is the effective spin mixing conductance at the YIG/NM interfaces which includes the spin current backflow driven by spin accumulation, g, $\mu_{\rm B}$, M_s ($4\pi M_s = 1794$ Oe [11]), and $t_{\rm YIG}$ are the Landé g factor, Bohr magneton, saturation magnetization, and thickness of the YIG layer, respectively. Rapid spin flips relax the injected spin very quickly in good spin sink materials such as Pt and W, preventing any backflow that results from spin accumulation, thus $g^{\uparrow\downarrow}_{\rm eff} \approx g^{\uparrow\downarrow}$. However, in NMs with slower relaxation, such as Cu [4,5],

$$g^{\uparrow\downarrow}_{\rm eff} = g^{\uparrow\downarrow}_{\rm YIG/NM}\left[1 + g^{\uparrow\downarrow}_{\rm YIG/NM}\frac{1}{4\sqrt{\frac{\epsilon}{3}\tanh\left(\frac{t_{\rm NM}}{\lambda_{\rm SD}}\right)}g^{\rm Sh}_{\rm NM}}\right]^{-1}, \tag{4}$$

where $g^{\uparrow\downarrow}_{\rm YIG/NM}$, $g^{\rm Sh}_{\rm NM}$, and ϵ are the "intrinsic" spin mixing conductance of the YIG/NM interface, Sharvin conductance of the NM, and the spin-flip probability of the NM [4,5].

The spin accumulation in Cu leads to backflow into the YIG so $g^{\uparrow\downarrow}_{\rm eff}$ is much smaller than $g^{\uparrow\downarrow}_{\rm YIG/Cu}$ depending on $t_{\rm NM}$ and ϵ. For YIG/Cu/NM trilayers where the NM is a spin sink, in the limit of vanishing spin flip in Cu [31,32], the effective spin mixing conductance $g^{\uparrow\downarrow}_{\rm eff,trilayer}$ of the trilayer is simply the serial contributions of the two interfaces and the spin resistance of Cu,

$$\frac{1}{g^{\uparrow\downarrow}_{\rm eff,trilayer}} = \frac{1}{g^{\uparrow\downarrow}_{\rm YIG/Cu}} + R_{\rm Cu} + \frac{1}{g_{\rm Cu/NM}}, \tag{5}$$

where the spin resistance $R_{\rm Cu} = \frac{2e^2 t_{\rm Cu}}{h\sigma}$ (σ is the electrical conductivity) [4,5]. Using measured resistivity of 4.0×10^{-8} Ωm for 20-nm Cu, we obtain $R_{\rm Cu} = 6.2 \times 10^{-20}$ m^2. In order to quantitatively determine the intrinsic $g^{\uparrow\downarrow}_{\rm YIG/Cu}$, we grow a 2-$\mu$m ($\gg \lambda_{\rm SD}$) Cu layer on YIG to reduce the backflow of spin current. Figure 3(c) shows the Gilbert damping enhancement of two YIG/Cu bilayers compared to a bare YIG film. The values of $\alpha_{\rm sp}$ for YIG/Cu(10 nm) and YIG/Cu(2 μm) are $(1.1 \pm 0.1) \times 10^{-4}$ and $(18 \pm 1) \times 10^{-4}$, respectively, clearly indicating significant backflow of spin current driven by spin accumulation when $t_{\rm Cu} \ll \lambda_{\rm SD}$. This is confirmed by FMR measurement shown in Fig. 3(f), where the linewidth change for YIG/Cu(2 μm) is 8.7 Oe, much larger than the 1.2 Oe for YIG/Cu(10 nm). From the value of $\alpha_{\rm sp}$, we obtain $g^{\uparrow\downarrow}_{\rm eff} = (3.4 \pm 0.3) \times 10^{18}$ m^{-2} for the YIG/Cu(2 μm) bilayer. From Eqs. (2)–(4) and using $\epsilon = 1/68$ and $\lambda_{\rm SD} = 245$ nm for Cu [31], we

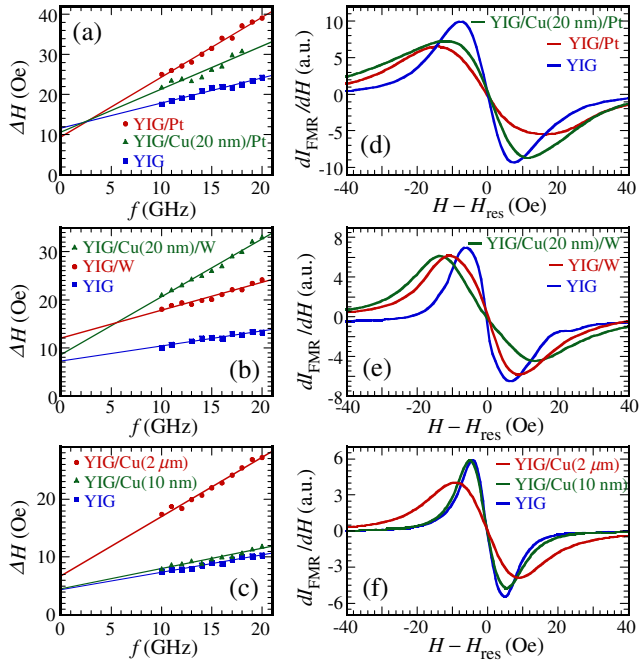

FIG. 3. Frequency dependencies of FMR linewidths of (a) YIG/Cu/Pt, (b) YIG/Cu/W, and (c) YIG/Cu series with corresponding FMR derivative absorption spectra at $f =$ 9.65 GHz shown in (d), (e), and (f).

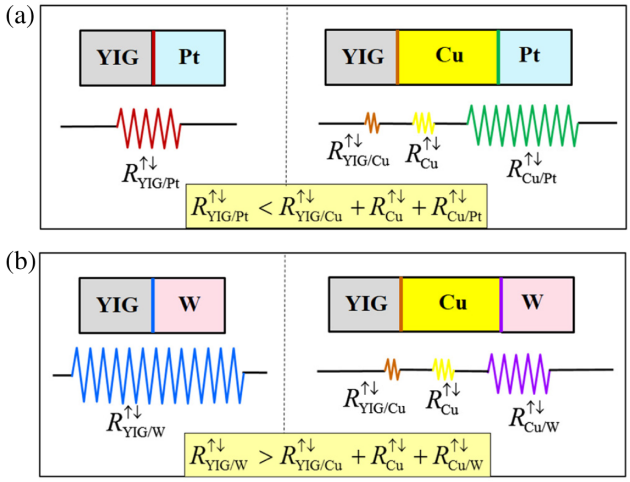

FIG. 4. Schematic comparison of spin mixing resistance or spin resistance of (a) YIG/Pt (red), YIG/Cu (brown), and Cu/Pt (green) interfaces, and (b) YIG/W (blue), YIG/Cu (brown), and Cu/W (purple) interfaces. The calculated values of spin mixing conductances explain the opposite behavior in Figs. 2(f) and 2(g): the insertion of a Cu layer suppresses the magnitude of spin current from YIG to Pt, but enhances the spin current generation from YIG to W.

calculate the intrinsic $g^{\uparrow\downarrow}_{YIG/Cu} = (1.8 \pm 0.2) \times 10^{19}$ m^{-2} for the YIG/Cu(2 μm) bilayer. As demonstrated in Ref. [31], the $g^{\uparrow\downarrow}_{eff,trilayer}$ of the YIG/Cu(20 nm)/Pt and YIG/Cu(20 nm)/W trilayers can be obtained from the damping enhancement using Eq. (3) by replacing $g^{\uparrow\downarrow}_{eff}$ with $g^{\uparrow\downarrow}_{eff,trilayer}$, from which we calculate the spin conductance $g_{Cu/Pt} = (2.8 \pm 0.4) \times 10^{18}$ m^{-2} which is smaller than $g^{\uparrow\downarrow}_{YIG/Pt} = (3.9 \pm 0.3) \times 10^{18}$ m^{-2}, and $g_{Cu/W} = (7.6 \pm 0.9) \times 10^{18}$ m^{-2} which is much larger than $g^{\uparrow\downarrow}_{YIG/W} = (1.2 \pm 0.1) \times 10^{18}$ m^{-2}.

Using the spin mixing conductances and spin conductance calculated above for each interface in the YIG/Cu/Pt and YIG/Cu/W trilayers, we can understand the opposite behavior of spin currents shown in Figs. 2(f) and 2(g). Figure 4 schematically shows the series circuits of spin current flow from YIG → Pt (or W) and from YIG → Cu → Pt (or W). Here, we use spin mixing resistance $R^{\uparrow\downarrow}_{YIG/NM} = 1/g^{\uparrow\downarrow}_{YIG/NM}$ to represent each YIG/NM interface and spin resistance $R_{Cu/NM} = 1/g_{Cu/NM}$ for each Cu/NM interface (Table I). For the YIG/Cu(20 nm)/Pt trilayer, the total spin resistance $R^{\uparrow\downarrow}_{YIG/Cu/Pt} = R^{\uparrow\downarrow}_{YIG/Cu} + R_{Cu} + R_{Cu/Pt} = (0.56 + 0.62 + 3.6) \times 10^{-19}$ m^2 $= 4.8 \times 10^{-19}$ m^2, larger than $R^{\uparrow\downarrow}_{YIG/Pt} = 2.6 \times 10^{-19}$ m^2 for YIG/Pt. As a result, the spin current at $t_{Cu} \geq 10$ nm is smaller (20%–25%) than $J_s(0)$ for YIG/Pt [Fig. 2(f)]. One notes that, relative to the YIG/Cu interface, the Cu/Pt interface is the dominant barrier to spin transport in the trilayer. For YIG/

TABLE I. Spin pumping parameters of bilayers and trilayers in this study: spin pumping enhanced damping $\alpha_{sp} = \alpha_{YIG/NM} - \alpha_{YIG}$ or $\alpha_{sp} = \alpha_{YIG/Cu/NM} - \alpha_{YIG}$ effective spin mixing conductance $g^{\uparrow\downarrow}_{eff}$ or $g^{\uparrow\downarrow}_{eff,trilayer}$ spin mixing conductance $g^{\uparrow\downarrow}_{YIG/NM}$ at YIG/NM interfaces, spin conductance $g_{Cu/NM}$ at Cu/NM interfaces, spin mixing resistance $R^{\uparrow\downarrow}_{YIG/NM} = 1/g^{\uparrow\downarrow}_{YIG/NM}$ at YIG/NM interfaces, spin resistance $R_{Cu/NM} = 1/g_{Cu/NM}$ at Cu/NM interfaces, and total spin mixing resistance $R^{\uparrow\downarrow}_{trilayer} = 1/g^{\uparrow\downarrow}_{eff,trilayer}$ for the trilayers.

Structure	α_{sp}	$g^{\uparrow\downarrow}_{eff}$ (m^{-2})	$g^{\uparrow\downarrow}_{eff,trilayer}$ (m^{-2})	$g^{\uparrow\downarrow}_{YIG/NM}$ (m^{-2})	$g_{Cu/NM}$ (m^{-2})	$R^{\uparrow\downarrow}_{YIG/NM}$ or $R_{Cu/NM}$ (m^{-2})	$R^{\uparrow\downarrow}_{trilayer}$ (m^{-2})
YIG/Pt	$(2.1 \pm 0.1) \times 10^{-3}$	$(3.9 \pm 0.3) \times 10^{18}$		$(3.9 \pm 0.3) \times 10^{18}$		$(2.6 \pm 0.2) \times 10^{-19}$	
YIG/W	$(6.3 \pm 0.6) \times 10^{-4}$	$(1.2 \pm 0.1) \times 10^{18}$		$(1.2 \pm 0.1) \times 10^{18}$		$(8.3 \pm 0.9) \times 10^{-19}$	
YIG/Cu(2 μm)	$(1.8 \pm 0.1) \times 10^{-3}$	$(3.4 \pm 0.3) \times 10^{18}$		$(1.8 \pm 0.2) \times 10^{19}$		$(5.6 \pm 0.5) \times 10^{-20}$	
YIG/Cu(20 nm)/Pt	$(1.1 \times 0.1) \times 10^{-3}$		$(2.1 \times 0.3) \times 10^{18}$				$(4.8 \pm 0.7) \times 10^{-19}$
YIG/Cu(20 nm)/W	$(2.1 \pm 0.2) \times 10^{-3}$		$(4.0 \pm 0.4) \times 10^{18}$				$(2.5 \pm 0.3) \times 10^{-19}$
Cu/Pt					$(2.8 \pm 0.4) \times 10^{18}$	$(3.6 \pm 0.5) \times 10^{-19}$	
Cu/W					$(7.6 \pm 0.9) \times 10^{18}$	$(1.3 \pm 0.2) \times 10^{-19}$	

Cu(20 nm)/W, the total spin resistance $R^{\uparrow\downarrow}_{\mathrm{YIG/Cu/W}} = R^{\uparrow\downarrow}_{\mathrm{YIG/Cu}} + R_{\mathrm{Cu}} + R_{\mathrm{Cu/W}} = (0.56 + 0.62 + 1.3) \times 10^{-19}\ \mathrm{m}^2 = 2.5 \times 10^{-19}\ \mathrm{m}^2$, smaller than $R^{\uparrow\downarrow}_{\mathrm{YIG/W}} = 8.3 \times 10^{-19}\ \mathrm{m}^2$ for YIG/W [Fig. 4(b)]. This is why the spin current plateau for YIG/Cu/W is approximately 4.5 times larger than $J_s(0)$ for YIG/W as shown in Fig. 2(g).

In summary, we systematically studied FMR spin pumping in YIG/Cu/Pt and YIG/Cu/W trilayers as well as YIG/Cu bilayers. Significant enhancement of spin currents is observed in YIG/Cu/W trilayers as compared to YIG/W bilayers with direct contact. From the spin pumping enhancement of Gilbert damping, we determined the spin mixing conductances of YIG/Pt, YIG/W, YIG/Cu interfaces, and spin conductances of Cu/Pt and Cu/W interfaces. These values explain the suppression of spin currents pumped into Pt in YIG/Cu/Pt trilayers and the enhancement of spin currents in YIG/Cu/W trilayers. This discovery potentially paves a path toward significant improvement of spin pumping efficiency by engineering multilayers with optimized spin conductance matching of the interfaces, a powerful capability for future spin-functional devices.

This work is supported by the Center for Emergent Materials at The Ohio State University, a NSF Materials Research Science and Engineering Center (No. DMR-0820414) (H. L. W. and F. Y. Y.) and by the U.S. Department of Energy through Grant No. DE-FG02-03ER46054 (P. C. H.). Partial support is provided by Lake Shore Cryogenics Inc. (C. H. D.) and the NanoSystems Laboratory at The Ohio State University. C. H. D. and H. L. W. have contributed equally to this work.

[1] I. Žutić, J. Fabian, and S. Das Sarma, Spintronics: Fundamentals and applications, Rev. Mod. Phys. **76**, 323 (2004).
[2] D. D. Awschalom and M. E. Flatté, Challenges for semiconductor spintronics, Nat. Phys. **3**, 153 (2007).
[3] J. Chow, R. J. Kopp, and P. R. Portney, Energy resources and global development, Science **302**, 1528 (2003).
[4] Y. Tserkovnyak, A. Brataas, G. E. W. Bauer, and B. I. Halperin, Nonlocal magnetization dynamics in ferromagnetic heterostructures, Rev. Mod. Phys. **77**, 1375 (2005).
[5] Y. Tserkovnyak, A. Brataas, and G. E. W. Bauer, Spin pumping and magnetization dynamics in metallic multilayers, Phys. Rev. B **66**, 224403 (2002).
[6] Y. Kajiwara, K. Harii, S. Takahashi, J. Ohe, K. Uchida, M. Mizuguchi, H. Umezawa, H. Kawai, K. Ando, K. Takanashi, S. Maekawa, and E. Saitoh, Transmission of electrical signals by spin-wave interconversion in a magnetic insulator, Nature (London) **464**, 262 (2010).
[7] B. Heinrich, C. Burrowes, E. Montoya, B. Kardasz, E. Girt, Y.-Y. Song, Y. Y. Sun, and M. Z. Wu, Spin pumping at the magnetic insulator (YIG)/normal metal (Au) interfaces, Phys. Rev. Lett. **107**, 066604 (2011).
[8] K. Ando, S. Takahashi, J. Ieda, H. Kurebayashi, T. Trypiniotis, C. H. W. Barnes, S. Maekawa, and E. Saitoh, Electrically tunable spin injector free from the impedance mismatch problem, Nat. Mater. **10**, 655 (2011).
[9] M. V. Costache, M. Sladkov, S. M. Watts, C. H. van der Wal, and B. J. van Wees, Electrical detection of spin pumping due to the precessing magnetization of a single ferromagnet, Phys. Rev. Lett. **97**, 216603 (2006).
[10] F. D. Czeschka, L. Dreher, M. S. Brandt, M. Weiler, M. Althammer, I.-M. Imort, G. Reiss, A. Thomas, W. Schoch, W. Limmer, H. Huebl, R. Gross, and S. T. B. Goennenwein, Scaling behavior of the spin pumping effect in ferromagnet-platinum bilayers, Phys. Rev. Lett. **107**, 046601 (2011).
[11] H. L. Wang, C. H. Du, Y. Pu, R. Adur, P. C. Hammel, and F. Y. Yang, Large spin pumping from epitaxial $Y_3Fe_5O_{12}$ thin films to Pt and W layers, Phys. Rev. B **88**, 100406(R) (2013).
[12] C. H. Du, H. L. Wang, Y. Pu, T. L. Meyer, P. M. Woodward, F. Y. Yang, and P. C. Hammel, Probing the spin pumping mechanism: Exchange coupling with exponential decay in $Y_3Fe_5O_{12}$/barrier/Pt heterostructures, Phys. Rev. Lett. **111**, 247202 (2013).
[13] C. Hahn, G. de Loubens, O. Klein, M. Viret, V. V. Naletov, and J. Ben Youssef, Comparative measurements of inverse spin Hall effects and magnetoresistance in YIG/Pt and YIG/Ta, Phys. Rev. B **87**, 174417 (2013).
[14] S. Mizukami, Y. Ando, and T. Miyazaki, Effect of spin diffusion on Gilbert damping for a very thin permalloy layer in Cu/permalloy/Cu/Pt films, Phys. Rev. B **66**,104413 (2002).
[15] C. Burrowes, B. Heinrich, B. Kardasz, E. A. Montoya, E. Girt, Y. Sun, Y.-Y. Song, and M. Wu, Enhanced spin pumping at yttrium iron garnet/Au interfaces, Appl. Phys. Lett. **100**, 092403 (2012).
[16] P. Deorani and H. Yang, Role of spin mixing conductance in spin pumping: Enhancement of spin pumping efficiency in Ta/Cu/Py structures, Appl. Phys. Lett. **103**, 232408 (2013).
[17] K. Uchida, S. Takahashi, K. Harii, J. Ieda, W. Koshibae, K. Ando, S. Maekawa, and E. Saitoh, Observation of the spin Seebeck effect, Nature (London) **455**, 778 (2008).
[18] T. Kikkawa, K. Uchida, Y. Shiomi, Z. Qiu, D. Hou, D. Tian, H. Nakayama, X.-F. Jin, and E. Saitoh, Longitudinal spin Seebeck effect free from the proximity Nernst effect, Phys. Rev. Lett. **110**, 067207 (2013).
[19] A. A. Serga, A. V. Chumak, and B. Hillebrands, YIG magnonics, J. Phys. D **43**, 264002 (2010).
[20] Y. Sun, Y.-Y. Song, H. Chang, M. Kabatek, M. Jantz, W. Schneider, M. Wu, H. Schultheiss, and A. Hoffmann, Growth and ferromagnetic resonance properties of nanometer-thick yttrium iron garnet films, Appl. Phys. Lett. **101**, 152405 (2012).
[21] S. M. Rezende, R. L. Rodríguez-Suárez, and A. Azevedo, Magnetic relaxation due to spin pumping in thick ferromagnetic films in contact with normal metals, Phys. Rev. B **88**, 014404 (2013).
[22] S. Y. Huang, X. Fan, D. Qu, Y. P. Chen, W. G. Wang, J. Wu, T. Y. Chen, J. Q. Xiao, and C. L. Chien, Transport magnetic proximity effects in platinum, Phys. Rev. Lett. **109**, 107204 (2012).

[23] Y. Sun, H. Chang, M. Kabatek, Y.-Y. Song, Z. Wang, M. Jantz, W. Schneider, M. Wu, E. Montoya, B. Kardasz, B. Heinrich, S. G. E. te Velthuis, H. Schultheiss, and A. Hoffmann, Damping in yttrium iron garnet nanoscale films capped by platinum, Phys. Rev. Lett. **111**, 106601 (2013).

[24] H. Nakayama, M. Althammer, Y.-T. Chen, K. Uchida, Y. Kajiwara, D. Kikuchi, T. Ohtani, S. Geprägs, M. Opel, S. Takahashi, R. Gross, G. E. W. Bauer, S. T. B. Goennenwein, and E. Saitoh, Spin Hall magnetoresistance induced by a nonequilibrium proximity effect, Phys. Rev. Lett. **110**, 206601 (2013).

[25] H. L. Wang, C. H. Du, P. C. Hammel, and F. Y. Yang, Strain-tunable magnetocrystalline anisotropy in epitaxial $Y_3Fe_5O_{12}$ thin films, Phys. Rev. B **89**, 134404 (2014).

[26] K. Ando, S. Takahashi, J. Ieda, Y. Kajiwara, H. Nakayama, T. Yoshino, K. Harii, Y. Fujikawa, M. Matsuo, S. Maekawa, and E. Saitoh, Inverse spin-Hall effect induced by spin pumping in metallic system, J. Appl. Phys. **109**, 103913 (2011).

[27] E. Shikoh, K. Ando, K. Kubo, E. Saitoh, T. Shinjo, and M. Shiraishi, Spin-pump-induced spin transport in *p*-type Si at room temperature, Phys. Rev. Lett. **110**, 127201 (2013).

[28] S. S. Kalarickal, P. Krivosik, M. Wu, C. E. Patton, M. L. Schneider, P. Kabos, T. J. Silva, and J. P. Nibarger, Ferromagnetic resonance linewidth in metallic thin films: Comparison of measurement methods, J. Appl. Phys. **99**, 093909 (2006).

[29] A. Kapelrud and A. Brataas, Spin pumping and enhanced Gilbert damping in thin magnetic insulator films, Phys. Rev. Lett. **111**, 097602 (2013).

[30] X. Jia, K. Liu, K. Xia, and G. E. W. B. Bauer, Spin transfer torque on magnetic insulators, Europhys. Lett. **96**, 17005 (2011).

[31] B. Kardasz and B. Heinrich, Ferromagnetic resonance studies of accumulation and diffusion of spin momentum density in Fe/Ag/Fe/GaAs(001) and Ag/Fe/GaAs(001) structures, Phys. Rev. B **81**, 094409 (2010).

[32] O. Mosendz, G. Woltersdorf, B. Kardasz, B. Heinrich, and C. H. Back, Magnetization dynamics in the presence of pure spin currents in magnetic single and double layers in spin ballistic and diffusive regimes, Phys. Rev. B **79**, 224412 (2009).

[33] A. Ghosh, S. Auffret, U. Ebels, and W. E. Bailey, Penetration depth of transverse spin current in ultrathin ferromagnets, Phys. Rev. Lett. **109**, 127202 (2012).